Pergamon

Int. J. Heat Mass Transfer. Vol. 39, No. 10, pp. 2015–2022, 1996

0017-9310/96 $15.00 + 0.00

0017-9310(95)00303-7

Turbulent forced convection in a helicoidal pipe with substantial pitch

G. YANG and M. A. EBADIAN†

Department of Mechanical Engineering, Florida International University, Miami, FL 33199, U.S.A.

(*Received* 24 *February* 1995 *and in final form* 2 *August* 1995)

Abstract—Fully developed turbulent convective heat transfer in a circular cross-section helicoidal pipe with finite pitch is numerically studied. The k-ε model is used to model the turbulent behavior. The time averaged momentum and energy equations are derived in the helicoidal coordinate system. The results indicate that the temperature distribution in the cross-section will be asymmetric as the pitch of the coil increases. Unlike that in laminar flow, an increase in the Prandtl number will reduce the torsion effect on the heat transfer in a helicoidal pipe. The results also indicate that the pitch effect will be enhanced as the flow rate increases. Copyright © 1996 Elsevier Science Ltd.

1. INTRODUCTION

Turbulent heat transfer in coiled pipes is commonly encountered in the design of compact heat exchangers, evaporators, combustors, and condensors used in the food, pharmaceutical, power and chemical industries. The convective turbulent heat transfer in coiled pipes has been experimentally studied by Jeschke [1], Woschni [2], and Rogers and Mayhew [3] for water and air. Petukhov and Popov [4], Schmidt [5] and Gnielinski [6] developed the correlation equations based on the test, and the derivation of the data from the correlation equation was less than $\pm 15\%$. Mori and Nakayama [7] applied boundary layer idealization to predict the temperature profile and heat transfer coefficient for the turbulent flow. Their calculated result was confirmed by their own experimental result.

To distinguish the differences in coiled pipes, the coiled pipe with a negligible pitch is usually termed as a *toroidal* pipe, and the coiled pipe with considerable pitch is designated as a *helicoidal* pipe. Although numerous studies have been conducted for toroidal pipe flow, only a limited number of papers has been published for the flow and heat transfer in a helicoidal pipe (the coiled pipe with considerable pitch). It is well known that the pitch of the coiled pipe will create an additional force—torsion—on the flow. The major obstacle for progress in this area of study is due mainly to the fact that the axial velocity in the helicoidal pipe is not orthogonal to the radial and tangential velocities in a helicoidal coordinate system. Wang [8] first introduced the nonorthogonal helicoidal coordinate to study the secondary flow in a helicoidal pipe. Murata *et al.* [9] simplified the Navier–Stokes equations by assuming a small curvature in a nonorthogonal coordinate system. Germano [10, 11] introduced a transformation to render the nonorthogonal coordinate system to an orthogonal one, and found that the effect of torsion on the secondary flow is second-order. Kao [12] used Germano's coordinate system to study the helicoidal pipe flow in a substantial range of Dean numbers using both perturbation and numerical methods. Recently, Xie [13], Tuttle [14], Chen and Jan [15], and Liu [16] tried to resolve the controversy between these researchers by linking Wang's coordinate system with Germano's coordinate system. Kao [12] and Yang *et al.* [17] studied the convective heat transfer in the helicoidal pipe with a finite pitch. However, all of these studies of the torsion effect on the flow and heat transfer in a helicoidal pipe were limited in the laminar flow region.

The above survey indicates that the theoretical and numerical studies on the forced convective heat transfer in the helicoidal pipe are limited in either the laminar region or the turbulent region with zero pitch. The objective of this study is to explore the effects of torsion on the fully developed turbulent forced convection in a helicoidal pipe with a finite pitch. In this study, the momentum and energy equations were derived in the helicoidal coordinate system as employed by Germano for laminar flow. The k-ε turbulent model, which has been successfully used in the toroidal pipe, has been applied to predict the turbulent viscosity. In the following sections, the governing equations in the helicoidal coordinates and the numerical procedures will be discussed, followed by a discussion of the results and conclusions.

2. THE GOVERNING EQUATIONS

The helicoidal coordinate system used by Germano [10] for laminar flow is applied in this study. In Fig.

† Author to whom correspondence should be addressed, Director, Hemispheric Center for Environmental Technology.

NOMENCLATURE

a	pipe diameter [m]
b	pitch [m]
C_1, C_2, C_μ	constant
De	Dean number
G	turbulent kinetic energy generation [$m^2 s^{-3}$]
k	kinetic energy [$m^2 s^{-2}$]
Pr	Prandtl number
Pr_t	turbulent Prandtl number
p	pressure [Nm^{-2}]
R	radius of the coil [m]
Re	Reynolds number
r	dimensionless radial direction coordinate [m]
s	dimensional axial coordinate [m]
T	temperature [°C]
u, v, w	velocity components [m s^{-1}]
$\mathbf{V}$	velocity [m s^{-1}]
w_b	dimensionless average axial velocity [m s^{-1}]
y_p	distance from the wall [m].

Greek symbols

α	angle
Γ	turbulent diffusivity
δ	dimensionless curvature, κa
ε	turbulent kinetic energy dissipation [$m^2 s^{-3}$]
θ	angle
κ	constant
λ	dimensionless torsion [$\tau\kappa^{-1}$]
μ	dynamic viscosity [kg $m^{-1} s^{-1}$]
ν	kinematic viscosity [$m^2 s^{-1}$]
ρ	density [kg m^{-3}]
σ_k, σ_ε	constants
τ	torsion; shear stress [$m^2 s^{-2}$]
Φ	general function
ψ	angle
ω	function.

Subscripts

b	bulk
k	turbulent kinetic energy
l	laminar
p	near boundary node
r	radial direction
s	axial direction
T	temperature
t	turbulent
ε	turbulent kinetic energy dissipation
ψ	tangential direction.

1, s indicates the dimensional axial coordinate, and $2a$ is the diameter of the circular cylinder in which s is coiled. R is the radius of the circular pipe, while r and $\psi = \theta + \phi$ are the coordinates in the radial and tangential directions, and b is the pitch of the helicoidal pipe. u, v and w are velocities in the tangential, radial and axial directions, respectively. The governing equations for fully developed flow can be written as

Continuity equation

$$\frac{1}{r}\frac{\partial u}{\partial \psi} + \frac{\partial v}{\partial r} + \frac{v}{r} + \delta\omega\left[u\cos\psi + v\sin\psi - \lambda\frac{\partial w}{\partial \psi}\right] = 0. \tag{1}$$

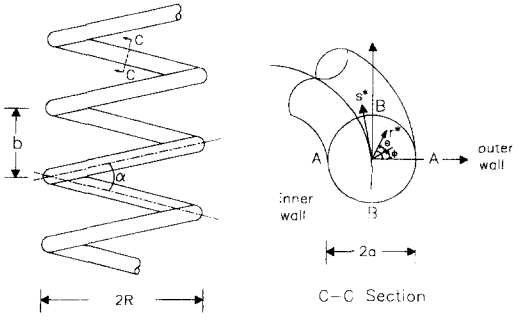

Fig. 1. The schematic of a helicoidal coordinate system.

Momentum equation

$$\rho\left(\frac{\partial(uu)}{r\partial\psi} + \frac{1}{r}\frac{\partial(ruv)}{\partial r}\right)$$
$$= -\frac{1}{r}\frac{\partial p}{\partial\psi} + \rho\delta w\omega\left(w\cos\psi + \lambda\frac{\partial u}{\partial\psi}\right)$$
$$-\rho\frac{uv}{r} - \rho u\delta\omega\left[u\cos\psi + v\sin\psi - \lambda\frac{\partial w}{\partial\psi}\right]$$
$$+\frac{1}{r}\frac{\partial}{\partial r}(r\tau_{r\psi}) + \frac{\partial}{r\partial\theta}(\tau_{\psi\psi}) + \frac{\tau_{r\psi}}{r}$$
$$+\delta\omega(\tau_{\psi\psi}\cos\psi + \tau_{r\psi}\sin\psi + \tau_{ss}\cos\psi)$$
$$-\delta\omega\lambda\frac{\partial}{\partial\psi}(\tau_{\psi s}) \tag{2}$$

$$\rho\left(\frac{1}{r}\frac{\partial(uv)}{\partial\psi} + \frac{1}{r}\frac{\partial(rvv)}{\partial r}\right)$$
$$= -\frac{\partial p}{\partial r} + \frac{1}{r}\frac{\partial(r\tau_{rr})}{\partial r} + \frac{1}{r}\frac{\partial(\tau_{r\psi})}{\partial\psi} + \rho\delta\omega w\Big)$$
$$\times\left(w\sin\psi + \lambda\frac{\partial v}{\partial\psi}\right) + \rho\frac{u^2}{r} - \rho v\delta\omega$$

$$\times\left[u\cos\psi+v\sin\psi-\lambda\frac{\partial w}{\partial\psi}\right]-\frac{\tau_{\psi\psi}}{r}+\delta\omega$$

$$\times(\tau_{r\psi}\cos\psi+\tau_{rr}\sin\psi-\tau_{ss}\sin\psi)-\delta\omega\lambda\frac{\partial}{\partial\psi}(\tau_{rs}) \tag{3}$$

$$\rho\left(\frac{\partial(uw)}{r\partial\psi}+\frac{1}{r}\frac{\partial(rvw)}{\partial r}\right)=-\omega\frac{\partial p}{\partial s}+2\rho w\delta\omega$$

$$\left[u\cos\psi+v\sin\psi-\lambda\frac{\partial w}{\partial\psi}\right]+\frac{1}{r}\frac{\partial}{\partial\psi}(\tau_{\psi s})$$

$$+\frac{1}{r}\frac{\partial}{\partial r}(r\tau_{rs})+2\delta\omega w(\tau_{\psi s}\cos\psi+\tau_{rs}\sin\psi). \tag{4}$$

Energy equation

$$\rho\left[\frac{1}{r}\frac{\partial(uT)}{\partial\psi}+\frac{1}{r}\frac{(rvT)}{\partial r}\right]$$

$$=\Gamma_T\left[\frac{1}{r^2}\frac{\partial^2T}{\partial\psi^2}+\frac{\partial^2T}{\partial r^2}+\frac{1}{r}\frac{\partial T}{\partial r}\right]$$

$$-\rho\omega w\frac{\partial T}{\partial s}-\rho T\left[\delta\omega\left(u\cos\psi+v\sin\psi-\lambda\frac{\partial w}{\partial\psi}\right)\right]$$

$$+\rho w\omega\delta\lambda\frac{\partial T}{\partial\psi}+\Gamma_T\left[\omega\delta\left(\frac{1}{r}\frac{\partial T}{\partial\psi}\cos\psi\right.\right.$$

$$\left.\left.+\frac{\partial T}{\partial r}\sin\psi\right)+\rho\lambda^2\delta^2\omega^2\left(\frac{\partial^2T}{\partial\psi^2}+\omega\delta r\cos\psi\frac{\partial T}{\partial\psi}\right)\right]. \tag{5}$$

Kinetic energy equation

$$\rho\left[\frac{1}{r}\frac{\partial(uk)}{\partial\psi}+\frac{1}{r}\frac{(rvk)}{\partial r}\right]=\frac{\Gamma_k}{\sigma_k}\left[\frac{1}{r^2}\frac{\partial^2k}{\partial\psi^2}+\frac{\partial^2k}{\partial r^2}\right.$$

$$\left.+\frac{1}{r}\frac{\partial k}{\partial r}\right]-\rho k\left[\delta\omega\left(u\cos\psi+v\sin\psi-\lambda\frac{\partial w}{\partial\psi}\right)\right]$$

$$+\rho w\omega\delta\lambda\frac{\partial k}{\partial\psi}+\frac{\mu_t}{\sigma_k}\left[\omega\delta\left(\frac{1}{r}\frac{\partial k}{\partial\psi}\cos\psi+\frac{\partial k}{\partial r}\sin\psi\right)\right.$$

$$\left.+\rho\lambda^2\delta^2\omega^2\left(\frac{\partial^2k}{\partial\psi^2}+\omega\delta r\cos\psi\frac{\partial k}{\partial\psi}\right)\right]+G-\rho\varepsilon. \tag{6}$$

Kinetic energy dissipation equation

$$\rho\left[\frac{1}{r}\frac{\partial(u\varepsilon)}{\partial\psi}+\frac{1}{r}\frac{(rv\varepsilon)}{\partial r}\right]=\frac{\Gamma_\varepsilon}{\sigma_\varepsilon}\left[\frac{1}{r^2}\frac{\partial^2\varepsilon}{\partial\psi^2}+\frac{\partial^2\varepsilon}{\partial r^2}\right.$$

$$\left.+\frac{1}{r}\frac{\partial\varepsilon}{\partial r}\right]-\rho\varepsilon\left[\delta\omega\left(u\cos\psi+v\sin\psi-\lambda\frac{\partial w}{\partial\psi}\right)\right]$$

$$+\rho w\omega\delta\lambda\frac{\partial\varepsilon}{\partial\psi}+\frac{\mu_t}{\sigma_\varepsilon}\left[\omega\delta\left(\frac{1}{r}\frac{\partial\varepsilon}{\partial\psi}\cos\psi+\frac{\partial\varepsilon}{\partial r}\sin\psi\right)\right.$$

$$\left.+\rho\lambda^2\delta^2\omega^2\left(\frac{\partial^2\varepsilon}{\partial\psi^2}+\omega\delta r\cos\psi\frac{\partial\varepsilon}{\partial\psi}\right)\right]+C_1\frac{\varepsilon}{k}G-\rho C_2\frac{\varepsilon^2}{k}. \tag{7}$$

In equations (2)–(4), τ_i represents the shear stress, which can be expressed in terms of velocity gradients and fluid viscosity

$$\tau_{\psi\psi}=2(\mu_l+\mu_t)\left(\frac{1}{r}\frac{\partial u}{\partial\psi}+\frac{v}{r}\right)$$

$$\tau_{rr}=2(\mu_l+\mu_t)\left(\frac{\partial v}{\partial r}\right)$$

$$\tau_{ss}=2(\mu_l+\mu_t)\left(-\omega\delta^2\lambda\frac{\partial w}{\partial\psi}+\omega\delta u\cos\psi+\omega\delta v\sin\psi\right)$$

$$\tau_{\psi r}=(\mu_l+\mu_t)\left[\frac{\partial w}{\partial r}-\omega\delta w\sin\psi-\omega\delta\lambda\frac{\partial v}{\partial\theta}\right]$$

$$\tau_{rs}=(\mu_l+\mu_t)\left(\frac{\partial w}{\partial r}-\omega\delta w\sin\psi-\omega\delta\lambda\frac{\partial v}{\partial\theta}\right)$$

$$\tau_{\psi s}=(\mu_l+\mu_t)\left(-\omega\delta^2\lambda\frac{\partial u}{\partial\psi}+\frac{1}{r}\frac{\partial w}{\partial\psi}-\omega\delta w\cos\psi\right). \tag{8}$$

In equations (5)–(7), Γ_i represents the diffusion coefficients of energy, the k and ε equations:

$$\Gamma_T=\frac{\mu_l}{Pr_l}+\frac{\mu_t}{Pr_t}$$

$$\Gamma_k=\mu_l+\frac{\mu_t}{\Gamma_k}$$

$$\Gamma_\varepsilon=\mu_l+\frac{\mu_t}{\Gamma_\varepsilon}. \tag{9}$$

In the equations, δ and λ represent the dimensionless curvature and torsion, respectively, and ω is a dimensionless function; they are defined as

$$\delta=\frac{aR}{R^2+b^2}$$

$$\lambda=\frac{b}{R}$$

$$\omega=\frac{1}{1+\delta r\sin\psi}. \tag{10}$$

The turbulent viscosity μ_t is modeled by:

$$\mu_t=C_\mu\rho\frac{k^2}{\varepsilon}, \tag{11}$$

and the constants recommended by Launder and Spalding [18] were used in this study

$$C_\mu=0.09,\quad C_1=1.47,$$

$$C_2=1.92,\quad \sigma_k=1.0,\quad \sigma_\varepsilon=1.3,\quad Pr_t=0.9.$$

The generation terms in the k and ε equations were calculated by $G=(\bar{\tau}\cdot\mathbf{V})\mathbf{V}$:

$$G=\mu_t\left\{2\left[\left(\frac{1}{r}\frac{\partial u}{\partial\theta}\right)^2+\left(\frac{v}{r}\right)^2+\left(\frac{\partial v}{\partial r}\right)^2+2\frac{v}{r^2}\frac{\partial u}{\partial\theta}\right.\right.$$

$$+\omega^2\left[\delta\omega\left(u\cos\psi+v\sin\psi-\lambda\frac{\partial w}{\partial\psi}\right)\right]^2-\frac{u}{r}\left(\frac{\partial v}{r\partial\theta}+\frac{\partial u}{\partial r}\right)-\omega\delta\lambda\left(\frac{1}{r}\frac{\partial u}{\partial\theta}\frac{\partial w}{\partial\theta}+\frac{\partial v}{\partial\theta}\frac{\partial w}{\partial r}\right)\Bigg]+\left(\frac{\partial v}{r\partial\theta}+\frac{\partial u}{\partial r}\right)^2+\left(\frac{u}{r}\right)^2+\left(\omega\delta\lambda\frac{\partial u}{\partial\theta}\right)^2+\left(\frac{1}{r}\frac{\partial w}{\partial\theta}\right)^2+(\omega\delta w)^2+\left(\frac{\partial w}{\partial r}\right)^2+\left(\omega\delta\lambda\frac{\partial w}{\partial\theta}\right)^2-2\omega\delta w\left[\cos\theta\left(\frac{1}{r}\frac{\partial w}{\partial\theta}-\omega\delta\lambda\frac{\partial u}{\partial\theta}\right)+\sin\theta\left(\frac{\partial w}{\partial r}-\omega\delta\lambda\frac{\partial v}{\partial\theta}\right)\right]\Bigg\}. \tag{12}$$

The wall function method has been used to specify the boundary conditions at the solid wall region. For radial velocity v the non-slip boundary condition was exposed. For the velocities in the tangential and axial directions, u and w,

$$\mu_t=\left[\frac{y(C_\mu^{1/4}k^{1/2})}{\nu}\right]\frac{\mu}{\ln(Ey^+)/\kappa}=\begin{cases}\dfrac{y^+\mu}{u^+}\,u\text{ velocity}\\[2ex]\dfrac{y^+\mu}{w^+}\,w\text{ velocity}\end{cases}$$

$$=\begin{cases}\mu & y^+\leqslant 11.5\\ \dfrac{\mu y^+}{2.5\ln(qy^+)} & y^+>11.5\end{cases}. \tag{13}$$

For the energy equation, the κ_t for the mode next to the wall can be written as

$$\Gamma_t=\begin{cases}\mu/P_{rt} & y^+\leqslant 11.5\\ \dfrac{\mu y^+}{Pr_t[2.5\ln(qy^+)+P]} & y^+>11.5\end{cases} \tag{14}$$

where

$$P=9\left(\frac{Pr}{Pr_t}-1\right)\left(\frac{Pr}{Pr_t}\right)^{-1/4}\cdot\frac{\mathrm{d}k}{\mathrm{d}r}\Big|_{r=a}=0$$

was used for the kinetic energy equation. Finally, the boundary condition of the dissipation of kinetic energy was given by specifying ε at the node next to the solid wall

$$\varepsilon_p=C_\mu^{3/4}k_p^{3/2}/\kappa y_p, \tag{15}$$

where the subscript p indicates the location at the node next to the solid wall, y_p is the distance between this node and the wall, and κ is a constant, $\kappa=0.4$.

Equations (1)–(7) are the governing equations of turbulent flow and heat transfer inside a helicoidal pipe. By setting the torsion equal to zero ($\lambda=0$), the above equations reduce to the governing equations in a toroidal pipe. Patankar *et al.* [19] have derived the governing equations for developing turbulent flow in the toroidal pipe. Comparison indicates that the reduced equation in this study ($\lambda=0$) is identical to Patankar's governing equations, if one sets the $\mathrm{d}\Phi/\mathrm{d}\phi$ term equal to zero in their study (Φ and ϕ are the general variable and axial coordinate, respectively).

The governing equations, equations (1)–(7), are nonlinear partial differential equations that have been solved by the *simple* algorithm (Patankar [20]). Four controlling parameters for the calculation are the axial pressure gradient, $\mathrm{d}p/\mathrm{d}s$, dimensionless curvature δ, torsion λ and Prandtl number Pr. The convergence criterion of

$$\frac{\|\Phi_{ij}^{k+1}-\Phi_{ij}^{k}\|}{\|\Phi_{ij}^{k+1}\|}\leqslant 10^{-5} \tag{16}$$

is applied for all equations, where Φ refers to u, v, w, p, T, k and ε. Subscripts i and j represent the arbitrary nodes, and superscript k represents the kth iteration. After the converged axial velocity has been obtained, the Reynolds number and the Dean number, the flow can be calculated by

$$Re=\frac{2\rho a w_b}{\mu_l}, \tag{17}$$

$$De=Re\delta^{1/2}, \tag{18}$$

where the bulk velocity w_b is

$$w_b=\frac{1}{\pi}\int_0^{2\pi}\int_0^1 wr\,\mathrm{d}r\,\mathrm{d}\psi, \tag{19}$$

$$T_b=\frac{2}{\pi w_b}\int_0^{\pi}\int_0^1 wTr\,\mathrm{d}r\,\mathrm{d}\theta. \tag{20}$$

A computer code was developed based on the above mentioned solution methodology. A grid refinement study was conducted in the present analysis to determine an adequate grid distribution. Uniform grid distributions (angular direction grids × radial direction grids) of 22×22, 30×30, 42×42, 50×50, 62×62 and 70×70 were tested. Table 1 is a comparison of the predicted results for fully developed Nusselt numbers at different grid distributions. An axial pressure gradient of $\mathrm{d}p/\mathrm{d}s/(\rho v^2/a)=-2\cdot10^6$, curvature of $\delta=0.025$, and Prandtl number of $Pr=0.7$ were applied during the calculation. The table indicates that the 62×62

Table 1. The predicted results with different grid arrangements

$L\times M$	Nu
22×22	119.8
30×30	114.4
42×42	117.5
50×50	119.9
62×62	121.6
70×70	121.8

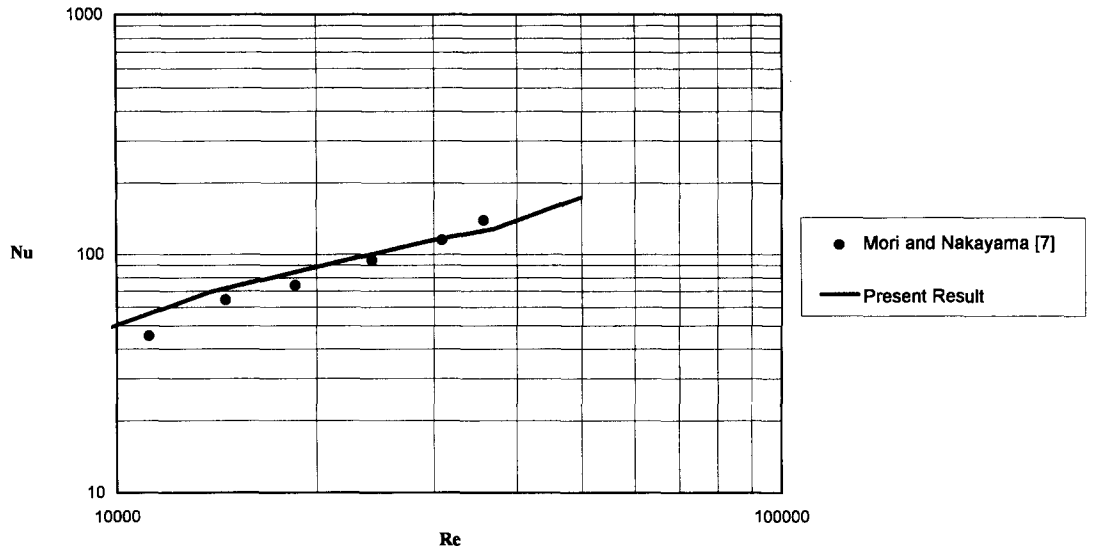

Fig. 2. Comparison of predicted results with the experimental results ($Pr = 0.7$).

grid arrangement ensures a satisfactory solution, and the results presented in this paper are based on the calculation of the 62×62 grid size distribution. In order to verify the accuracy of the computer code, the predicted results have been compared with the information in the open literature and Schmidt [5] for water. Figure 2 shows the comparison of the predicted results with the tested results of Mori and Nakayama [7] for air. The curvature of the helix was $\delta = 0.025$, and the calculation was based on $Pr = 0.7$. The figure indicates that the predicted results agree very well with the tested data. Figure 3 gives another comparison for water. In the figure, the open box indicates the test results from Schmidt [5], and the cross indicates the results from Rogers and Mayhew [3]. The solid line represents the results from the prediction of Petukhov and Popov [4], while the dot indicates the results from the present study. The figure demonstrates that the predicted results agree well with Rogers and Mayhew at a low Reynolds number range ($Re < 20\,000$) and were close to the Schmidt results when the Reynolds number was larger than 20 000.

3. RESULTS AND DISCUSSION

Since the enhancement of heat transfer in a curved pipe with a finite pitch is strongly dependent on the behavior of the secondary flow in the cross-section, the temperature distribution and corresponding secondary flow patterns will be discussed simultaneously. Figure 4 shows the effects of torsion on the fluid temperature and secondary flow patterns in a helicoidal pipe. During the calculation, $R/a = 40$ and the dimensionless axial pressure gradient, $\mathrm{d}p/\mathrm{d}s/(\rho v^2/a) = -2.10^6$, have been applied. The torsion, λ, changes from 0 to 0.5. The Reynolds numbers in the three cases are around 30 000, which ensures that the flow is in the turbulent region. Figure 4a illustrates the time averaged secondary velocity distribution in the cross-section of a toroidal pipe when $\lambda = 0$. Due to the unbalanced centrifugal force generated by the primary flow, the fluid flows outward in the center region of the pipe and returns to the innermost point along the solid wall. Since $\lambda = 0$, the two vortices are symmetric to the centerline between the outermost points to the innermost point of the pipe. Figure 4b shows the temperature distribution for a fluid when $Pr = 0.7$ (air). Due to the secondary flow, the temperature contours with high values were pushed toward the outer wall region, as in laminar flow (Yang and Ebadian [17]). The temperature contours were symmetric to the centerline between the innermost point and the outermost point. Figure 4c indicates a very similar temperature distribution behavior as that in Fig. 4b for the fluid when $Pr = 5.0$ (water). However, the temperature in the $Pr = 5.0$ fluid was much more uniform than in air.

Figures 4d–i exhibit the time averaged secondary velocity and temperature distributions in a helicoidal pipe with a finite coil pitch, while the torsion λ is 0.1 and 0.5. As torsion is applied, Fig. 4d, g shows that the two vortices of the secondary flow in both cases become symmetrical. The vortex in the top region is enlarged and the one in the bottom region has shrunk. The profile distortion is enhanced as torsion increases. Since torsion is a rotational force that will generate a rotational flow, when both centrifugal force and torsion are applied, this rotational flow will enlarge the tangential velocity in one vortex and reduce it in another. Figures 4e, 4f, 4h and 4i show the temperature distributions in both cases, indicating the temperature contours rotate clockwise and are distorted. The distortion and rotations of the temperature contours will increase as torsion increases.

Table 2 shows the torsion effect on Nusselt numbers in a helicoidal pipe. During the calculation, $R/a = 40$, and the dimensionless axial pressure gradient,

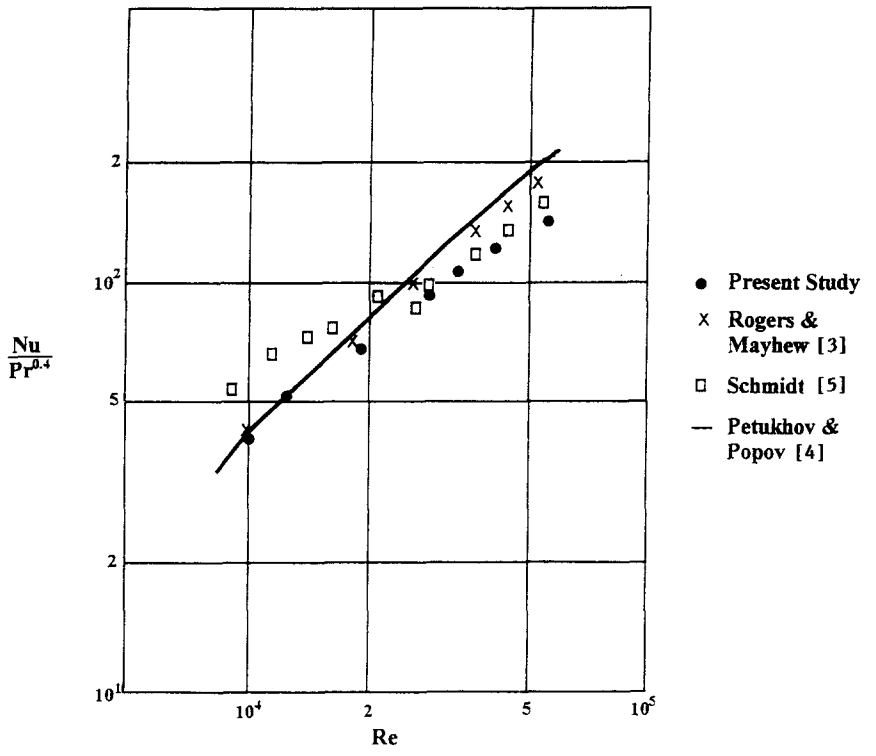

Fig. 3. Comparison of Nusselt number for water ($Pr = 5$).

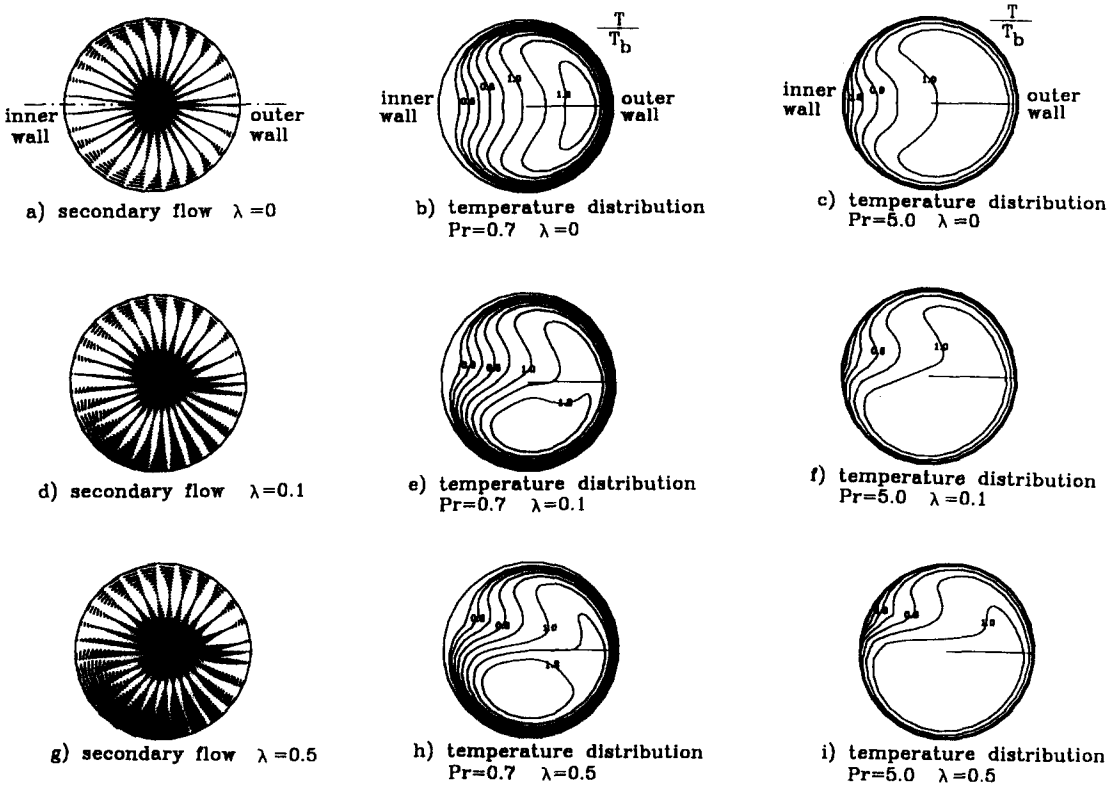

Fig. 4. The secondary flow and temperature distribution in a cross-section of helicoidal pipe.

Table 2. Effect of torsion on the heat transfer rate for $Re = 3 \times 10^6$

		$Pr = 0.7$		$Pr = 5.0$	
λ	α	Nu	$Nu/Nu_{\lambda=0}$	Nu	$Nu/Nu_{\lambda=0}$
0	0	114.1	1.0	190.6	1.0
0.1	17.8°	117.8	1.032	194.1	1.018
0.2	34.9°	120.1	1.053	197.0	1.034
0.3	50.4°	121.1	1.061	197.7	1.037
0.5	76.3°	122.0	1.069	197.5	1.036
0.7	95.4°	122.5	1.074	196.2	1.029
1.0	115.0°	123.4	1.082	192.8	1.012

Table 3. Effect of torsion on the heat transfer behavior at different flow rates

	$Pr = 0.7$			$Pr = 5.0$		
Re	$\lambda = 0$	$\lambda = 0.3$	$\lambda = 1.0$	$\lambda = 0$	$\lambda = 0.3$	$\lambda = 1.0$
$2 \cdot 10^4$	88.0	90.1	90.8	133.3	135.5	132.0
$3 \cdot 10^4$	114.1	121.1	123.4	190.6	197.7	192.8
$5 \cdot 10^4$	151.6	175.4	180.3	285.6	314.8	305.2

$dp/ds/(\rho v^2/a) = -2 \cdot 10^6$ have been applied. The Reynolds number is around $3 \cdot 10^6$, and the torsion changed from 0 to 1, which, corresponding to the angle, α (as seen in Fig. 1), varied from 0 to 115°. For air, $Pr = 0.7$, the Nusselt number will be slightly increased with torsion. When torsion increases from 0 to 0.5, the Nusselt number increases around 7%. As torsion increases further, the increase in the Nusselt number becomes much slower. For water, $Pr = 5.0$, the Nusselt number increases as torsion increases in the beginning. The Nusselt number increases 3.7%, when the torsion increases to 0.3, then the Nusselt number gradually decreases. Table 3 indicates the effect of torsion on the heat transfer behavior at different flow rates. At a low rate, $Re = 20\,000$, the torsion effect is not significant for both air and water. At this flow rate. the Nusselt number changes less than 3% as the torsion varies from 0 to 1.0. However, at a large flow rate, $Re = 50\,000$, the Nusselt number changes significantly, especially for air. Table 3 also shows the same behavior as in Table 2 of water. As torsion increases, the Nusselt number increases at the beginning, and then reduces.

Figure 5 shows the comparison of the temperature distributions between the laminar flow and turbulent flow, with both cases having the same Prandtl number and torsion. It can be seen that the cold fluid has penetrated deeply in the center region, and divided the high temperature contours into two separated islands. In the turbulent flow region, this cold fluid penetration was minor. There are two reasons behind this phenomena. First, the ratio of secondary primary velocities of the turbulent region is much smaller than that of the laminar flow region. Second, the turbulent thermal diffusivity in turbulent is much larger than that in laminar flow. For example, when $Re = 30\,000$, the turbulent thermal diffusivity is around 40 times higher than that of laminar flow. Due to the difference of temperature distribution, the heat transfer behavior of turbulent flow is totally different from that of laminar flow. For example, when Pr. 0.7, the Nusselt will increase 6.1%, when torsion increases from zero to 0.3 in turbulent region ($Re = 30\,000$). However, the Nusselt number will average 8.0% with the same Prandtl number, and torsion changes when $Re = 400$.

4. CONCLUSION

Fully developed turbulent flow and convective heat transfer in a circular cross-section helicoidal pipe with finite pitch is numerically studied in this paper. The time averaged momentum and energy equations, as well as the k and ε equations, have been derived in the helicoidal coordinate system. The k-ε model is used to model the turbulent kinetic energy and its dissipation rate. The predicted heat transfer rates for both water and air compare well with available experimental test results. The results indicate that torsion will rotate

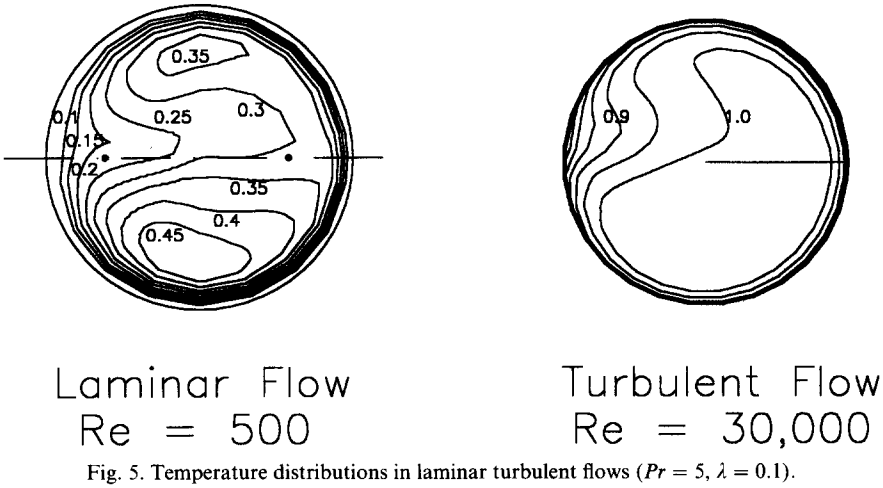

Fig. 5. Temperature distributions in laminar turbulent flows ($Pr = 5$, $\lambda = 0.1$).

and distort the temperature contours in the cross-section as in laminar flow. For air, the Nusselt number will increase as torsion increases. However, for water, the Nusselt number will increase with torsion in the beginning, and then it will decrease. The results indicate that unlike that of laminar flow, the torsion effect on the heat transfer will decrease with the Prandtl number. The results also show that the effect of torsion will be enhanced by an increase in the fluid axial flow rate.

Acknowledgement—The results presented in this paper were obtained in the course of research sponsored by the National Science Foundation under grant no. CTS-9017732.

REFERENCES

1. H. Jeschke, Warmeubergang und druckverlust in rohrsclangen, *beih. Techn. Mech. zur Zeitschr. d. VDI* **69,** 24–28 (1925).
2. G. Woschni, Untersuchung des warmeubergangs und des Druckverlusts in gekrummten rohren ; Dr.-Ing. Diss. TH Dresden, DDR (1959).
3. G. F. C. Rogers and Y. R. Mayhew, Heat transfer and pressure loss in helically coiled tubes with turbulent flow, *Int. J. Heat Mass Transfer* **7,** 1207–1216 (1964).
4. B. S. Petukhov and V. N. Popov, Theoretical calculation of heat exchange and frictional resistance in turbulent flow in tubes of an incompressible fluid with variable physical properties, *High Temp.* **1,** 69–83 (1963).
5. E. F. Schmidt, Warmeubergang und druckverlust in Rohrschlangen, *Chemie-Ing.-Techn.* **36,** 781–789 (1967).
6. V. Gnielinski, Correlation for the pressure drop in helicoidal coiled tubes, *Int. Chem. Engng* **26,** 36–44 (1986).
7. Y. Mori and W. Nakayama, Study on forced convective heat transfer in curved pipes (2nd Report, Turbulent Region), *Int. J. Heat Mass Transfer* **10,** 37–59 (1967).
8. C. Y. Wang, On the low-reynolds number flow in a helical pipe, *J. Fluid Mech.* **108,** 185–194 (1981).
9. S. Murata, Y. Miyake, T. Inaba and H. Ogawa, Laminar flow in a helically coiled pipe, *Bull. JSME* **24,** 355–362 (1981).
10. M. Germano, On the effect of torsion in a helical pipe flow, *J. Fluid Mech.* **125,** 1–8 (1982).
11. M. Germano, The dean equations extended to a helical pipe flow, *J. Fluid Mech.* **203,** 289–356 (1989).
12. H. C. Kao, Torsion effect on fully developed flow in a helical pipe, *J. Fluid Mech.* **184,** 335–356 (1987).
13. D. G. Xie, Torsion effect on secondary flow in a helicoidal pipe, *Int. J. Heat Fluid Flow* **111,** 114–119 (1990).
14. E. R. Tuttle, Laminar flow in twisted pipes, *J. Fluid Mech.* **219,** 545–570 (1990).
15. W. H. Chen and R. Jan, The characteristics of laminar flow in a helicoidal circular pipe, *J. Fluid Mech.* **244,** 241–256 (1992).
16. S. Liu, Laminar flow and heat transfer in helical pipes with finite pitch, Ph.D. Dissertation, University of Alberta (1992).
17. G. Yang, Z. Dong and M. A. Ebadian, Convective heat transfer in a helicoidal pipe heat exchanger, *ASME Trans. J. Heat Transfer* **115,** 796–800 (1993).
18. B. E. Launder and D. B. Spalding, *Mathematical Models of Turbulence*. Academic Press, London (1972).
19. S. V. Patankar, V. S. Pratap and D. B. Spalding, Prediction of turbulent flow in curved pipes, *J. Fluid Mech.* **67,** 583–595 (1975).
20. S. V. Patankar, *Numerical Heat Transfer and Fluid Flow*. Hemisphere, Washington, D.C. (1980).